A novel elastic-body-rotation model for concrete cover spalling caused by non-uniform corrosion of reinforcement

Ray Kai Leung Su[1], Yanlong Zhang

Department of Civil Engineering, The University of Hong Kong, Pokfulam Road, Hong Kong, PRC

Abstract: A novel elastic-body-rotation model is proposed to analyze the mechanism and the process of cover cracking and spalling caused by the non-uniform corrosion of widely spaced reinforcements. The width of the cover surface cracks, bulging of the concrete surface and maximum thickness of the corroded steel can be predicted by using the proposed model. The predicted bulging of the concrete cover has been validated by the experimental and numerical results. Using the validated model, the effects of the diagonal crack angle, tensile strength of concrete and cover thickness on the bulging of the cover surface and the thickness of the corroded steel for initiating and widening cracks are investigated with a parametric study. It is found that the diagonal cracking angle has a major influence on the cover surface crack width. In addition, the degree of corrosion in rebars and the width of internal diagonal cracks can be evaluated by simply measuring the width of surface cracks or the bulging of cover surface.

Keywords: Concrete cover; Non-uniform corrosion; Cover spalling; Analytical model

1. Introduction

Steel corrosion in reinforced concrete (RC) elements has been identified as one of the most predominant problems in the deterioration of concrete structures worldwide [1-4] as the durability, serviceability, and strength of RC structures are adversely affected by corrosion induced concrete cracking, spalling and cover delamination [5-13]. Experimental studies have found that in environments with a large concentration of chloride, there is more rust on the side of the rebars that are near the cover surface [14-17], which is mainly caused by macrocell corrosion of the rebars [18-23]. A number of non-uniform corrosion models [24-44] have been proposed to study cover cracking induced by this kind of corrosion and generally, the literature discusses two kinds of non-uniform corrosion in RC structures [26, 41]: rust that is non-uniformly distributed around the cross section of steel or along the rebars [45]. In this study, non-uniform corrosion refers to the former.

Callahan et al. [46] and Bazǎnt [47] suggested that corrosion induced cracking could be diagonal cracks when the cover thickness is relatively small or the spacing of the rebars is relatively wide. In such configurations, the crack patterns of RC structures

[1] Corresponding author. Tel.:+852 2859 2648
E-mail address: klsu@hku.hk (RKL Su)

due to the non-uniform corrosion of the rebars [27-29, 33, 48-51] usually consist of two diagonal cracks (about 40°-65° normal to the cover surface) together with a single crack that is perpendicular to the cover as shown in Fig. 1a. A slab with a spalled cover is shown in both an illustration and a photo in Figs. 1b and 1c, respectively. However, the deterioration mechanism of concrete covers due to the non-uniform corrosion of rebars is still unclear. Even though the thickness of corroded steel and the width of diagonal cracks and cover surface cracks are the three key parameters for investigating the amount and rate of corrosion, as well as the residual service life of RC structures, it is still difficult to directly measure the first two parameters. Also, merely estimating the service life of structures based on the width of surface cracks is an unreliable method [52]. Some numerical methods [29, 41, 48, 49] have been developed to study the relationships among these three parameters, yet they are relatively complex and difficult to implement by practicing engineers and designers. Therefore, it is imperative to develop a simple analytical model to simulate the deterioration mechanism of concrete covers and predict the thickness of corroded steel due to the non-uniform corrosion of the rebars.

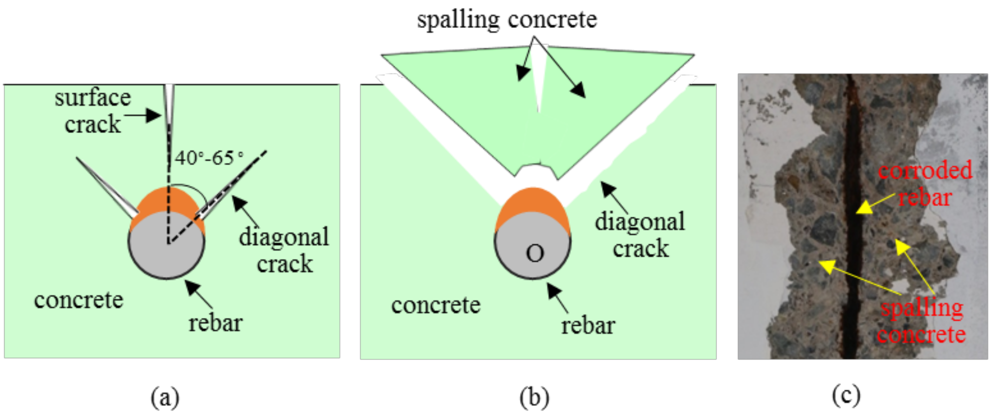

Fig. 1 Non-uniform corrosion of rebar which causes (a) cover cracking, (b) cover spalling, and (c) cover spalling (on a slab)

In this study, a novel elastic-body-rotation (EBR) model is proposed to study the deterioration mechanism and spalling process of concrete covers caused by the non-uniform corrosion of widely-spaced multiple rebars in RC slabs or walls. Elastic stands for elastic deformation, body stands for concrete body and rotation is the rotation of the concrete body. Furthermore, the numerical results obtained from a nonlinear finite element analysis carried out by using ATENA are used to validate the predicted results from the proposed model. Lastly, a parametric study is carried out by using the validated model to examine the effects of the diagonal crack angle, tensile strength of concrete and cover thickness on the bulging of the concrete surface and the thickness of the corroded steel in initiating and widening diagonal cracks and cover surface cracks.

2. Elastic-body-rotation model for concrete cover spalling

In this section, an analytical model that takes into consideration the elastic deformation of concrete to simulate the mechanism of cover cracking due to the non-uniform corrosion of widely spaced rebars is discussed. The term ‘widely spaced’ means that the rebar spacing is wide enough so that there is sufficient clearance from neighboring rebars that are corroded which mitigates their influence.

2.1 Distribution of rust

For simplicity and computational efficiency, the problem in this study is modelled based on a two dimensional approach. The distribution of non-uniform rust is assumed to be in a crescent shape [14] as shown in Fig. 2 in which D is the diameter of the rebar, $d_{\mathrm{s,max}}$ is the maximum thickness of the corroded steel, and $d_{\mathrm{r,max}}$ is the maximum thickness of the rust. The area of the corroded steel, V_{steel}, can be expressed as:

$$V_{\mathrm{steel}} = \frac{1}{2}\frac{\pi D^2}{4} - \frac{1}{2}\frac{\pi D}{2}\left(\frac{D}{2} - d_{\mathrm{s,max}}\right) = \frac{\pi D d_{\mathrm{s,max}}}{4} \quad (1)$$

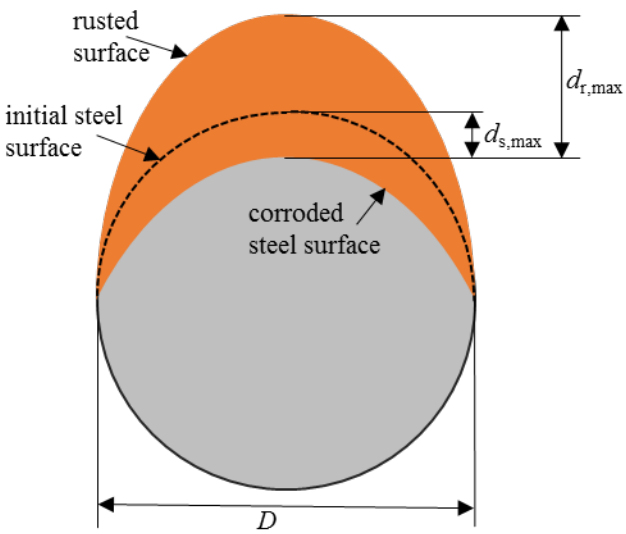

Fig. 2 Distribution of non-uniform rust in a crescent shape

2.2 Mechanism of cover cracking

At the steel/concrete interface, the expansion pressure caused by the corrosion of the rebars on the side near the cover will push against the concrete cover and cause the concrete bodies ABIC and ABI′C′ to rotate about the pivot points, C and C′, as shown in Fig. 3a, where Points B, I and I′ are all located at the steel/concrete interface [53]. Such deformations lead to tensile stress concentration at Points A, I and I′ and concentrated compressive stresses at Points B, C and C′ [28, 53], as shown in Fig. 3b. Diagonal cracks will initiate when the tensile stress reaches the tensile strength of concrete [27-29, 33, 48-50]. After that, the two symmetrically oriented diagonal cracks will propagate toward the cover surface along IC and I′C′, respectively, as shown in Fig. 3a [27]. Furthermore, a single crack that is perpendicular to the cover surface will initiate when the tensile stress reaches the tensile strength of concrete as shown in Fig. 3a. The crack will propagate along Line AB toward the corroded steel [29]. It should be noted that this surface crack will not penetrate through the entire cover as the concrete near the steel/concrete interface (i.e. Point B) is in compression [28, 48, 49]. Eventually, the diagonal cracks along IC and I′C′ will cause cover spalling when they reach the cover surface as shown in Fig. 3c [27, 46, 47]. The rotation of the concrete bodies could extend to the concrete surface beyond the region of C′C which is in compression as shown in Fig. 3b. Further details of the cover deterioration mechanism will be given in the numerical study in Section 4.1.

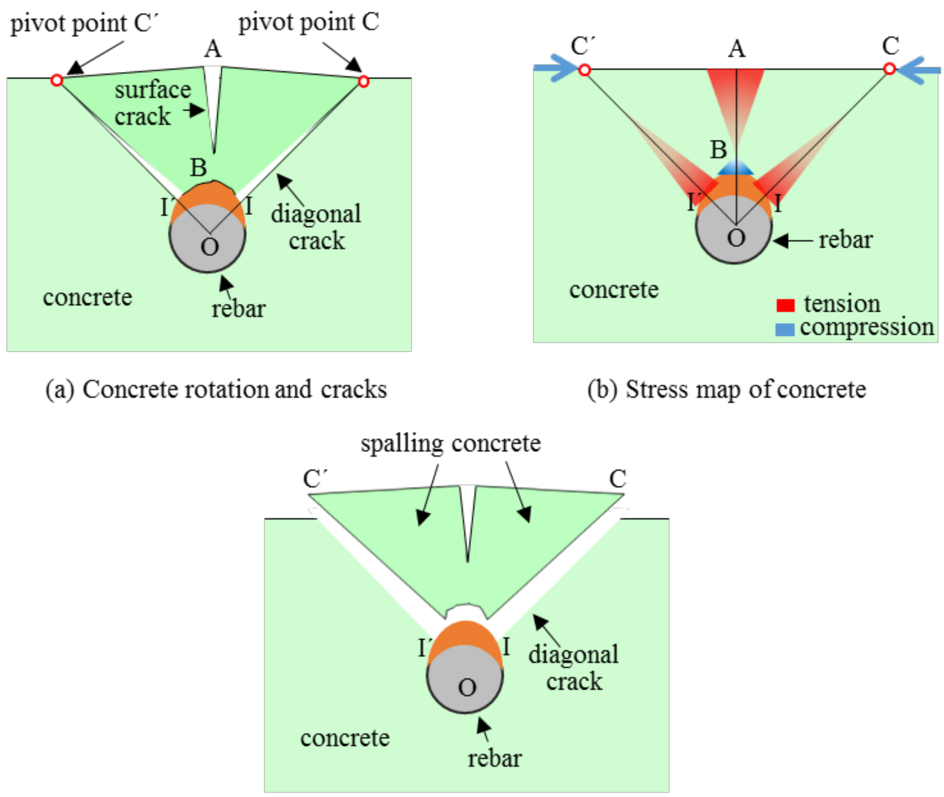

(a) Concrete rotation and cracks

(b) Stress map of concrete

(c) Cover spalling caused by diagonal cracks

Fig. 3 Elastic-body-rotation model for cover cracking caused by non-uniform corrosion of rebar

2.3 Corrosion expansion

As the corrosion of the rebars advances, the total area of rust is determined by considering [3, 5]: (1) the filled area of the corroded steel; (2) the area of rust penetration into the porous zone caused by entrapped or entrained air around the steel/concrete interface [54, 55], and (3) the level of expansion pressure at the steel/concrete interface caused by rust. Therefore, the total area of rust can be summarized as follows:

$$V_{\mathrm{rust}} = V_{\mathrm{steel}} + V_{\mathrm{porous}} + V_{\mathrm{net}} \tag{2}$$

where V_{rust} is the total area of rust, V_{steel} is the filled area of the corroded steel, V_{porous} is the area of rust that has penetrated into the porous zone and V_{net} is the net area of rust that induces expansion pressure onto the surrounding concrete. It should be noted that the amount of rust in corrosion-induced cracks is not taken into account here as the literature has not reached consensus on whether rust fills corrosion-induced cracks and if so, the amount of rust that fills the cracks [1, 34, 41, 56-64].

By defining β as the ratio of the amount of rust to corroded steel, the area of rust becomes:

$$V_{\mathrm{rust}} = \beta V_{\mathrm{steel}} \tag{3}$$

The relationship between $d_{\mathrm{s,max}}$ and $d_{\mathrm{r,max}}$ can be expressed as:

$$d_{\mathrm{r,max}} = \beta d_{\mathrm{s,max}} \tag{4}$$

For different components that are rusted, β may vary from 1.7 to 6.15 (FeO = 1.7, Fe_3O_4 = 2, Fe_2O_3 = 2.1, α-FeO(OH) = 2.95, β-FeO(OH) = 3.53, $Fe(OH)_2$ = 3.6, γ-FeO(OH) = 3.07, $Fe(OH)_3$ = 4.0, $Fe(OH)_3 3H_2O$ = 6.15) [2, 65] and experimental studies [66, 67] have found that β is about 3 for a rust mixture.

Some in the literature have pointed out [2, 3, 68, 69] that there is a porous zone around the interface between a rebar and concrete which can accommodate rust and therefore, prolong the time that the concrete cover is damaged through the expansion of rust. For non-uniform corrosion, it is reasonable to assume that rust is only deposited onto concrete that is adjacent to the corroding part, i.e. only the porous zone around the corroded steel accommodates rust [26]. Therefore, the area of rust that penetrates into the porous zone that surrounds one half of the rebar can be expressed as:

$$V_{\mathrm{porous}} = \frac{\pi d_0}{2}(D + d_0) \tag{5}$$

where d_0 is the thickness of the porous zone.

Liu and Weyers [2, 70] and Lu et al. [2, 70] hypothesized that the porous zone is first filled with rust and then further rusting would induce expansion pressure onto the surrounding concrete. However, other researchers [57, 71-73] postulate instead that the penetration of rust into concrete and the formation of a corrosion layer with expansion pressure take place at the same time. In this study, the assumptions of [2, 70] and [2, 70] are adopted. The thickness of the porous zone was assumed to be 12.5 µm ≤ d_0≤ 120 µm [2, 68, 70, 74, 75].

The maximum thickness of corroded steel that fills the porous zone, $d_{\mathrm{s,0,max}}$, around the corroded steel can be obtained by substituting Eqs. (1), (3) and (5) into Eq. (2)

$$d_{\mathrm{s,0,max}} = \frac{2d_0}{\beta - 1} \tag{6}$$

After filling up the porous zone with rust, the net maximum thickness of the rust $d_{f,max}$ (which is defined as the maximum thickness of rust that causes expansion pressure onto the surrounding concrete) can be obtained with:

$$d_{\mathrm{f,max}} = (\beta - 1)\left(d_{\mathrm{s,max}} - d_{\mathrm{s,0,max}}\right) \tag{7}$$

2.4 Displacement compatibility due to rotation of concrete cover

In this analytical model, the concrete bodies ABIC and ABI′C′ as shown in Fig. 3a are assumed to be symmetrical about Line AB. Points O, I and C are assumed to be collinear where O is the center of the rebar with no corrosion. By taking into consideration the rotation of elastic concrete bodies ABIC and ABI′C′, the crack opening displacement associated with concrete body rotation at Points I and A, which are denoted as $W_{I,R}$ and $W_{A,R}$ respectively, may be expressed as:

$$W_{\mathrm{I,R}} = \frac{d_{\mathrm{f,max}}(2L_{\mathrm{OC}} - D)}{2L_{\mathrm{AC}}} \tag{8}$$

$$W_{\mathrm{A,R}} = \frac{2d_{\mathrm{f,max}}c}{L_{\mathrm{AC}}} \tag{9}$$

where c is the thickness of the concrete cover and L_{OC} and L_{AC} are the length of OC and AC respectively, which can be expressed as:

$$L_{\mathrm{OC}} = \frac{D + 2c}{2\cos\varphi} \tag{10}$$

$$L_{\mathrm{AC}} = \left(\frac{D}{2} + c\right)\tan\varphi \tag{11}$$

where φ is the angle of the diagonal crack. The effects of the elastic deformation of the concrete bodies are taken into consideration but will be elaborated in Section 2.6.

2.5 Properties of materials

The elastic deformation of the rebars is neglected [70] in this study because the Young's modulus of steel (~200 GPa) is much higher than that of concrete (about 20-30 GPa). Therefore, the rebars are assumed to be rigid. Furthermore, the influence of the deformation of the rusted layer on calculating the amount of rust can also be neglected [3, 70, 76, 77] if the Young's modulus of the rust E_{rust} or the bulk modulus of the rust K_{rust} is high enough, for instance, $E_{rust} \geq 500$ MPa [3], $E_{rust} \geq 1$ GPa [70], $K_{rust} \geq 4$ GPa [76] or $K_{rust} \geq 300$ MPa [77]. For simplicity, rust is considered to be rigid in the analysis here. Furthermore, as no surface traction is applied on the concrete cover, the axial strain of the concrete cover in the direction normal to the cover surface is small and can be neglected. Hence, the bulging of the concrete cover at Points A and C, which are denoted as d_A and d_C, is equal to $d_{f,max}$ and zero, respectively. For simplicity, the bulging of concrete cover along AC is assumed to linearly decrease from $d_{f,max}$ to zero as shown in Fig. 4. Therefore, the bulging of the cover surface along AC, d_{cs}, can be expressed as:

$$d_{\mathrm{cs}} = \frac{L_{\mathrm{AC}} - x}{L_{\mathrm{AC}}} d_{\mathrm{f,max}} \tag{12}$$

where x is the horizontal coordinate with Point A as the origin.

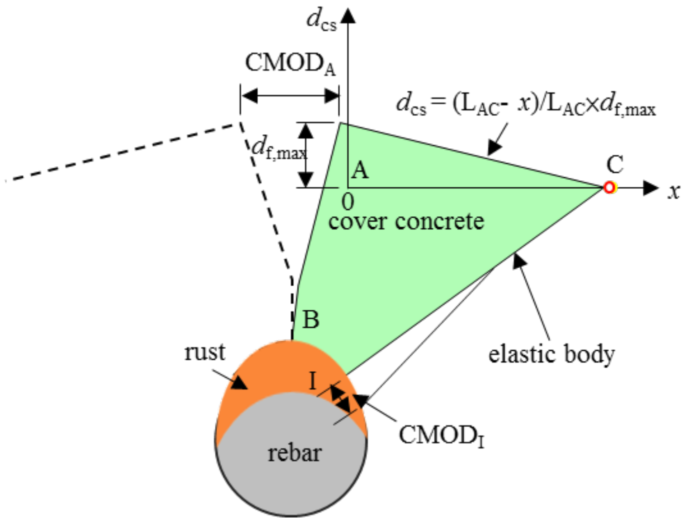

Fig. 4 Displacement of cracked cover

The linear elastic stress-strain relationship of concrete can be expressed as:

$$\varepsilon_{\mathrm{t}} = \frac{\sigma_{\mathrm{t}}}{E_{\mathrm{c,ef}}} \tag{13}$$

where ε_t is the tensile strain, σ_t is the tensile stress, $E_{\mathrm{c,ef}} = E_{\mathrm{c}}/1 - \phi_{\mathrm{ct}}$ is the effective elastic modulus of concrete, E_c is the elastic modulus of concrete and ϕ_{ct} is the creep coefficient of concrete.

When the tensile stress reaches the tensile strength of concrete (f_t), the corresponding concrete strain is:

$$\varepsilon_{\mathrm{ct}} = \frac{f_{\mathrm{t}}}{E_{\mathrm{c,ef}}} \tag{14}$$

2.6 Concrete cracking criterion

In this study, the tangential strain of concrete around the corroded rebar at the steel-concrete interface is assumed to be uniform [2, 43, 78] before cover cracking. Furthermore, two diagonal cracks initiate at Points I (and I′) when $W_{\mathrm{I,R}}$ reaches the critical elastic deformation limit of concrete in tension, i.e.,

$$W_{\mathrm{I,Ec}} = W_{\mathrm{I,R}} = \frac{\pi D \varepsilon_{\mathrm{ct}}}{2} \tag{15}$$

where $W_{\mathrm{I,Ec}}$ is the critical elastic displacement of concrete at Point I (and I′).

Along Line AC, the horizontal tensile stress of concrete at Point A is greater than that further away from this point; thereby it is reasonable to assume that the horizontal tensile strain of concrete decreases linearly from Points A to C [79]. This assumption will be justified by the finite element results provided in Section 4.1. At Point A, cover surface cracking takes place when $W_{A,R}$ is equal to the critical tensile strain of concrete multiplied by L_{AC}, i.e.,

$$W_{\mathrm{A,Ec}} = W_{\mathrm{A,R}} = 2L_{\mathrm{AC}}\frac{\varepsilon_{\mathrm{ct}}}{2} \tag{16}$$

where $W_{A,Ec}$ is the critical elastic horizontal displacement of concrete on the cover surface.

After the concrete cracks, the crack width will increase from zero as corrosion progresses. As shown in Fig. 4, the crack mouth opening displacement, $\mathrm{CMOD_I}$ and $\mathrm{CMOD_A}$ at Points I and A respectively can be expressed as:

$$\mathrm{CMOD_I} = W_{\mathrm{I,R}} - W_{\mathrm{I,Ec}} \tag{17}$$

$$\mathrm{CMOD_A} = W_{\mathrm{A,R}} - W_{\mathrm{A,Ec}} \tag{18}$$

The area of rust that will result in the initiation of diagonal cracks and cover surface cracks ($V_{\mathrm{steel,Ic}}$ and $V_{\mathrm{steel,Ac}}$), as well as the relationships between V_{steel} and $\mathrm{CMOD_A}$, V_{steel} and d_A and V_{steel} and $\mathrm{CMOD_I}$ which can be derived from Eqs. (1) to (18), are shown in Eqs. (19) to (23).

$$V_{\mathrm{steel,Ic}} = \frac{\pi D}{4(\beta-1)}\left\{\frac{\pi D f_{\mathrm{t}}(D+2c)\sin\varphi}{2E_{\mathrm{c,ef}}[D(1-\cos\varphi)+2c]} + 2d_0\right\} \tag{19}$$

$$V_{\mathrm{steel,Ac}} = \frac{\pi D}{4(\beta-1)}\left\{\frac{f_{\mathrm{t}}(D+2c)^2\tan\varphi^2}{8cE_{\mathrm{c,ef}}} + 2d_0\right\} \tag{20}$$

$$V_{\mathrm{steel}} = \frac{\pi D}{4(\beta-1)}\left\{\left(\frac{(D+2c)f_{\mathrm{t}}\tan\varphi}{2E_{\mathrm{c,ef}}} + \mathrm{CMOD_A}\right)\frac{(D+2c)\tan\varphi}{4c} + 2d_0\right\} \tag{21}$$

$$V_{\mathrm{steel}} = \frac{\pi D}{4(\beta-1)}(d_{\mathrm{A}} + 2d_0) \tag{22}$$

$$V_{\mathrm{steel}} = \frac{\pi D}{4(\beta-1)}\left\{\left(\frac{\pi D f_{\mathrm{t}}}{2E_{\mathrm{c,ef}}} + \mathrm{CMOD_I}\right)\frac{(D+2c)\sin\varphi}{D(1-\cos\varphi)+2c} + 2d_0\right\} \tag{23}$$

Eqs. (19) and (20) can be used to obtain the areas of corroded steel for the initiation of diagonal crack and cover surface crack, respectively. Eqs (21) and (22) can be used to obtain the areas of corroded steel with the measureable width of the cover surface cracks $\mathrm{CMOD_A}$, and bulging at Point A, d_A, respectively. Eq. (23) can be used to obtain the width of diagonal cracks $\mathrm{CMOD_I}$ with the area of corroded steel. By using Eqs. (19) to (23), readers would be able to determine the degree of corrosion of rebars and the width of internal diagonal crack based on the width of the cover surface crack or the bulging of cover surface.

3. Finite element simulation

The analytical model for cover cracking caused by rebar corrosion described in Section 2 is simulated with a finite element software called ATENA. Fig. 5 shows the schematic and boundary conditions of the concrete element with a cross section of 100 mm × 150 mm. The rebar is replaced with a hole that has a diameter of 20 mm. The stress distribution on the side near the cover decreases linearly with respect to the rust distribution while the stress distribution on the opposite side of the rebars is uniformly distributed [2, 78], which makes the force around the rebars equilibrium in the simulation. The cover thickness is 20 mm. A total of 1776 elements are used in this analysis. Concrete material is modeled with SBETA material model together with an exponential tension softening curve. SBETA is the abbreviation of StahlBETonAnalyse which means the analysis of reinforced concrete in German. Its peculiarities of the concrete model are that: (1) fracture of concrete in tension is based on the nonlinear fracture mechanics and (2) the tension stiffening effect and biaxial strength failure criterion have been considered. The concrete parameters adopted in the analysis are f_t = 2.317 MPa, $E_{c,ef}$ = 30.23 GPa, Poisson's ratio = 0.2 and specific fracture energy G_f = 57.93 N/m.

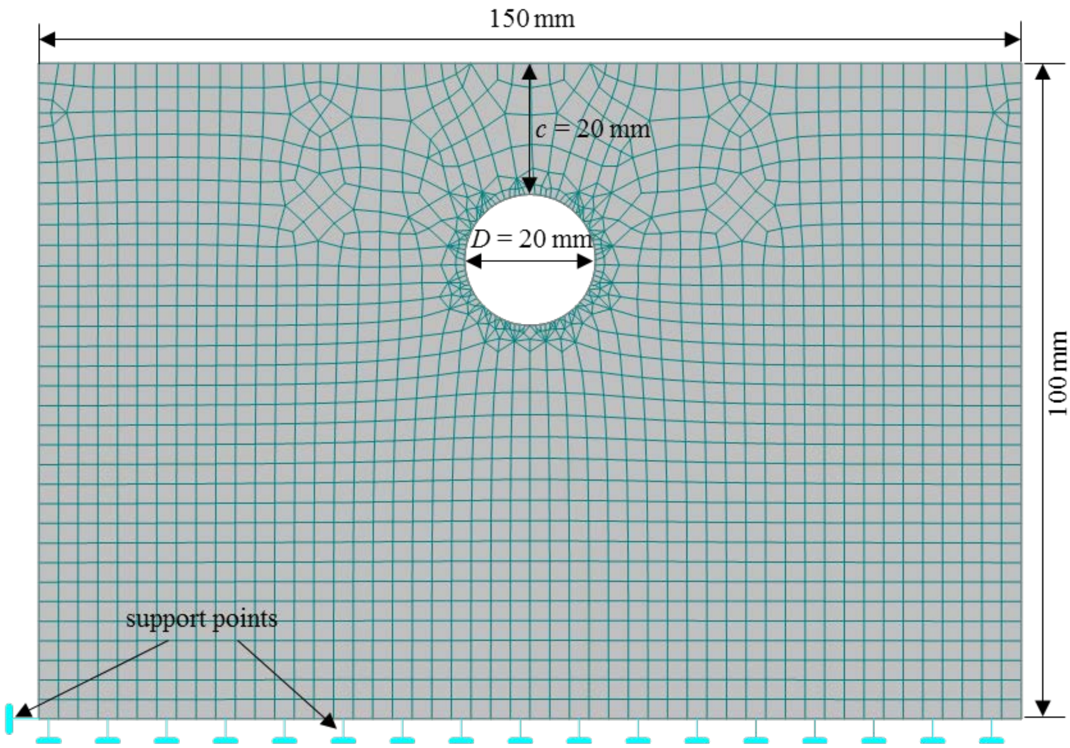

Fig. 5 Size and boundary conditions of concrete element with ATENA

4. Validation

4.1 Mechanism and cracking process of concrete cover

Fig. 6 shows the tensile stress distribution of the concrete along the diagonal crack (φ = 55°), the thinnest cover, and on the cover surface which is obtained from ATENA. It can be observed that, along the diagonal crack (I′C′), the tensile stress of the concrete near the steel/concrete interface is the highest at the beginning of the corrosion of the rebar when there is no cracking as shown in Fig. 6a. The diagonal crack first emerges when the tensile stress just reaches the tensile strength of the concrete as shown in Fig. 6b. With the accumulation of rust, the diagonal crack propagates toward the cover while residual tensile stress in the cracked concrete is as shown in Figs. 6c and 6d.

Along the thinnest cover (BA), the stress distribution of concrete is governed by two combined effects before cracking of the cover surface: (1) the elastic deformation of concrete which is caused by the expansion of rust and (2) the rotation of the concrete bodies. The expansion of rust causes greater tensile stress near the steel/concrete interface than on the cover surface, while the two concrete bodies press against each other near the steel/concrete interface and move in the opposite direction at the cover surface due to their rotation, which leads to concrete in compression near the steel/concrete interface and concrete in tension near the cover surface. The resultant stress distribution of the concrete along the thinnest cover that incorporates these two combined effects is shown in Fig. 6. When the tensile stress on the cover surface reaches the tensile strength of concrete, the surface crack initiates as shown in Fig. 6c, while the concrete near the steel/concrete interface is merely in compression. After cracking of the cover, the elastic deformation of concrete is reduced and the effect of the rotation of the concrete bodies dominates the deformation and displacement of the cracked cover. This leads to a higher compressive stress in the concrete near the steel/concrete surface and less tension in the concrete near the cover surface as shown in Fig. 6d.

Along Line AC', the horizontal tensile stress in the concrete slightly decreases from the crack mouth (Point A) to the pivot point (Point C') before cracking of the cover, which supports the assumed strain distribution as discussed in Section 2.6. Furthermore, the cover surface outside Line AC' is in compression during the cracking process of the cover and the compression stress increases with increases in the rotation of the concrete body $ABI'C'$ as shown in Fig. 6.

The stress distribution, as mentioned, is in good agreement with that adopted in the proposed EBR model and the findings of the analytical model on the cracking mechanism of the cover discussed in Section 2.2 are generally in line with those obtained from the finite element method. Furthermore, the cracking process of the concrete cover obtained from the proposed EBR model is also supported by the numerical results from ATENA. Both the analytical and the finite element models show that the diagonal cracking takes place before the cracking of the cover surface, which is also in agreement with the numerical results [29, 33, 48, 49]. The net maximum thickness of the rust $d_{f,max}$ for the initiation of diagonal and cover cracks obtained from the EBR model is 2.44 μm and 3.52 μm which is in close agreement with the results obtained by using ATENA, that is, 2.41 μm and 3.87 μm.

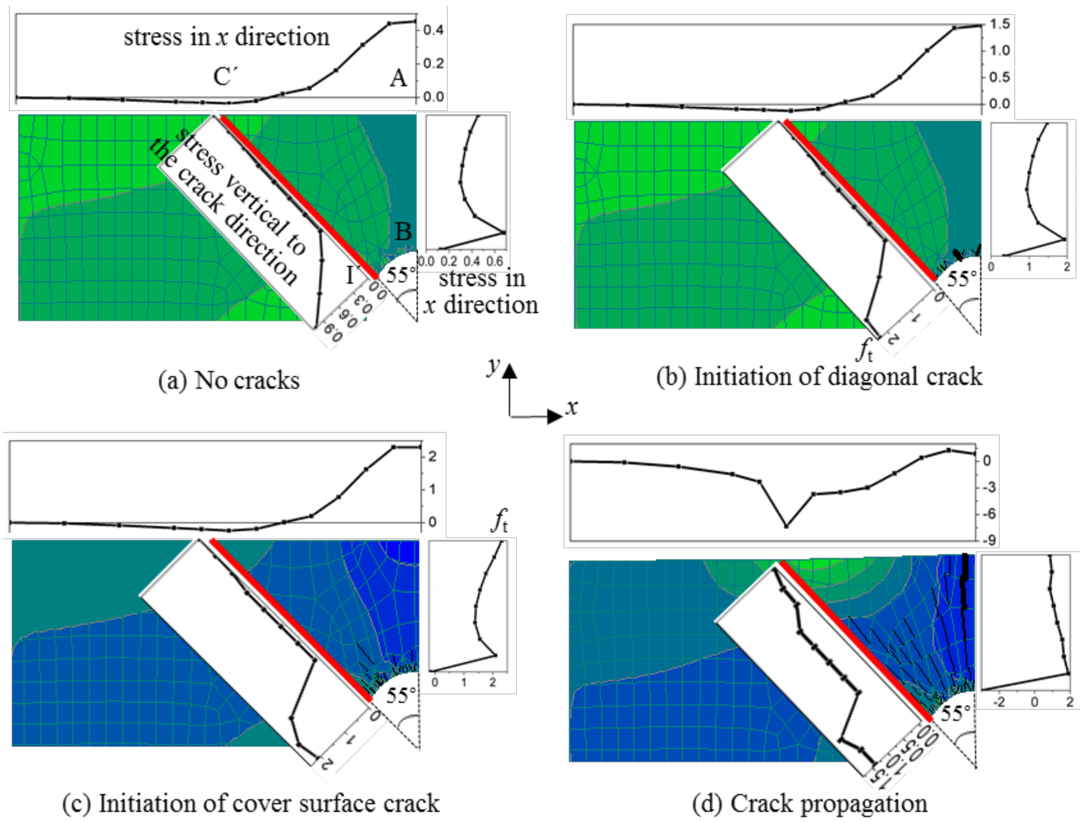

Fig. 6 Stress distribution of concrete along diagonal crack and thinnest cover and on the cover surface: (a) no cracks when $d_{f,max}$ = 0.741 μm; (b) Initiation of diagonal crack when $d_{f,max}$ = 2.41 μm; (c) Initiation of cover surface crack when $d_{f,max}$ = 3.87 μm; and (d) Crack propagation when $d_{f,max}$ = 18.1 μm

4.2 Bulging of cover surface

Tran et al. [34] experimentally evaluated the cracking behavior of concrete due to the non-uniform corrosion of a single rebar. The surface deformation and width of the surface crack were measured by using a laser displacement meter. Fig. 7 shows a comparison of the surface deformation evaluated by using the EBR model vs. testing [34]. It can be seen that the deformation shape and maximum deformation obtained from the EBR model are generally consistent with the experimental results. The small difference between the analytical and experimental results in Fig. 7c may be caused by the coarse aggregates in concrete which could affect the propagation direction of cracks.

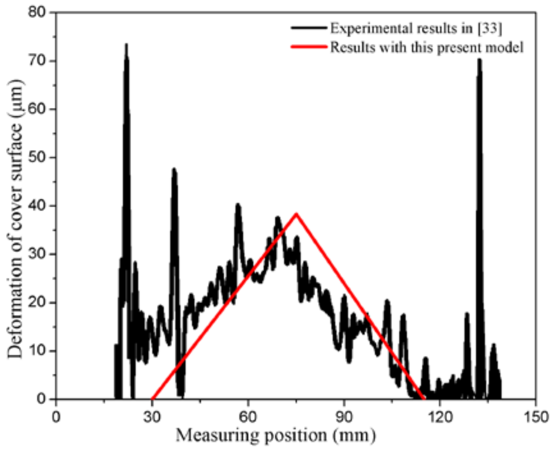

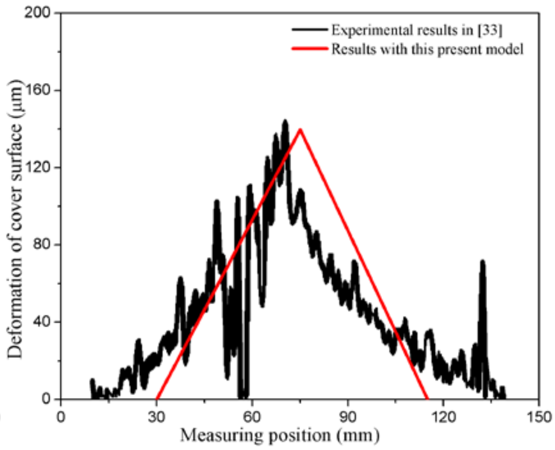

(a) (b)

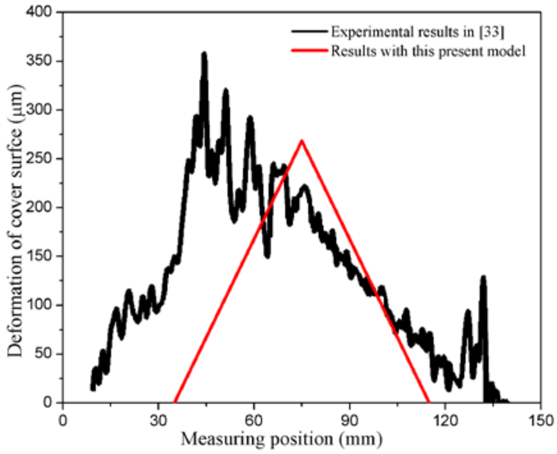

(c)

Fig. 7 Bulging of cover surface versus crack mouth opening displacement of surface crack: (a) $\mathrm{CMOD_A}$ = 54 μm, (b) $\mathrm{CMOD_A}$ = 208 μm and (c) $\mathrm{CMOD_A}$ = 403 μm (f_t = 1.53 MPa, $E_{c,ef}$ = 21.7 GPa, c = 30 mm, D = 19 mm, d_0 = 12.5 μm, β = 3, φ = 45°)

Fig. 8 is a comparison of the deformation of the cover surface determined by using the EBR model and ATENA for different net maximum thicknesses of rust. It can be observed that the shape of the deformation and maximum deformation determined by using the EBR model agree well with those obtained by using ATENA.

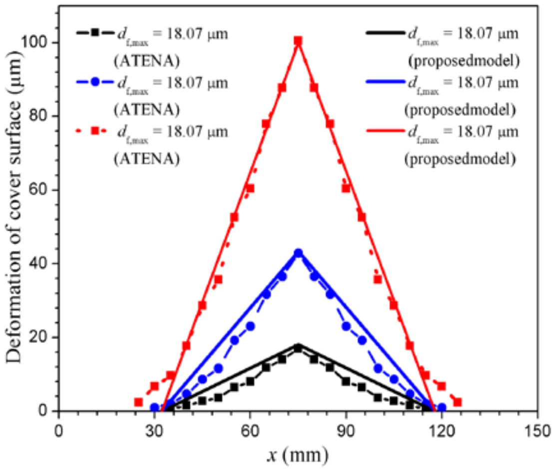

Fig. 8 Bulging of cover surface obtained with EBR model and ATENA

4.3 Thickness of corroded steel for crack initiation

Zhang et al. [29] investigated the cracking of a concrete cover resultant of the non-uniform corrosion of the rebars by using a damaged plasticity finite element model. Table 1 is a comparison of the results obtained from the EBR model vs. the model in Zhang et al. [29] of the net steel loss with the use of a ratio; that is, the ratio of the net area of corroded steel with the thickness of $d_{f,max}$ to the area of the rebar that has not been corroded, when diagonal cracks and cover surface cracks are initiated. It can be observed that the net steel loss ratios obtained with the EBR model agree very well with those obtained with the model in Zhang et al. [29] ($f_t = 0.5\sqrt{30} = 2.74$ MPa [80], $E_{c,ef} = 25.5$ GPa, $d_0 = 12.5$ μm, $\beta = 3.36$, $\varphi = 60°$).

Table 1 Net steel loss ratio (%) for initiation of diagonal crack and cover surface crack

c (mm)	D (mm)	diagonal crack at Point I		cover surface crack at Point A	
		EBR model	[29]	EBR model	[29]
35	16	0.0068	0.0065	0.0225	0.0285
	18	0.0069	0.0080	0.0212	0.0246
	20	0.0070	0.0061	0.0198	0.0219
	22	0.0070	0.0081	0.0188	0.0191
	25	0.0071	0.0087	0.0176	0.0167
	28	0.0072	0.0070	0.0167	0.0146
20	16	0.0077	0.0084	0.0167	0.0149
30		0.0070	0.0081	0.0205	0.0239
35		0.0069	0.0065	0.0225	0.0285

4.4 Cover surface cracking

Fig. 9 compares the crack mouth opening displacement on the cover surface obtained by using the EBR model and ATENA. It can be observed that the analytical results are in excellent agreement with the numerical results.

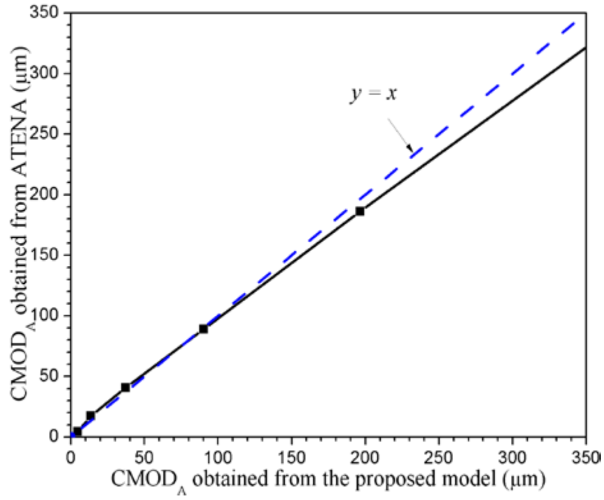

Fig. 9 Comparison of crack mouth opening displacement of surface crack obtained with EBR model and ATENA

5. Results and discussion

A parametric study is conducted by using the EBR model to investigate the effects of the diagonal crack angle, tensile strength of concrete and cover thickness on the bulging of concrete covers and the thickness of corroded steel for initiating and widening diagonal cracks and cover surface cracks. Furthermore, the variations in the bulging of the cover surface with an increase in the corrosion of the rebars are elaborated.

5.1 Effect of diagonal crack angle

The effects of the diagonal crack angle on the maximum thickness of the corroded steel for initiating and widening a diagonal crack and a cover surface crack are shown in Fig. 10. This figure shows that the maximum thickness of the corroded steel for the initiation of a diagonal crack and a cover surface crack increases with an increase in the diagonal crack angle, and for the same maximum thickness of corroded steel, a larger diagonal crack angle means a narrower diagonal crack and cover surface crack.

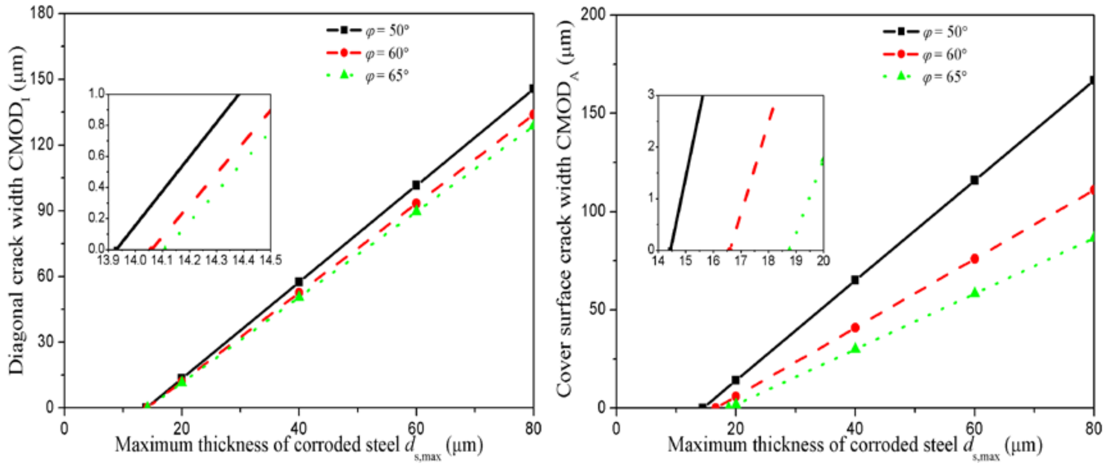

(a) Diagonal crack (b) Cover surface crack

Fig. 10 Effects of diagonal crack angle on initiating and widening (a) diagonal crack and (b) cover surface crack (f_t = 2.5 MPa, $E_{c,ef}$ = 20 GPa, c = 25 mm, D = 16 mm, d_0 = 12.5 μm and β = 3)

Fig. 11 shows the effect of the diagonal crack angle on the bulging of the cover surface. It can be seen that the variation in the diagonal crack angle has no effect on the maximum deformation of the concrete cover while the deformed area affected by the corrosion of steel increases as the diagonal crack angle increases.

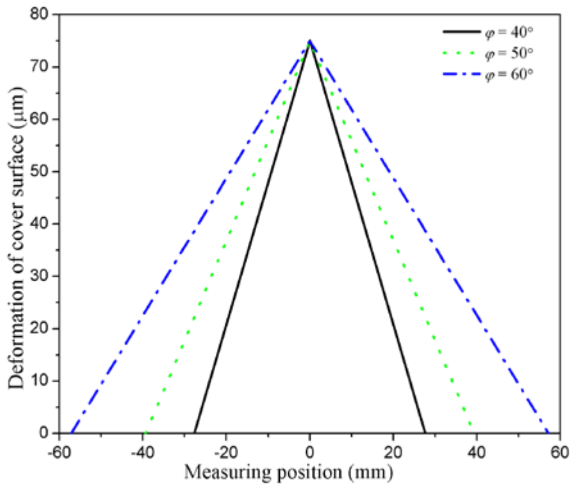

Fig. 11 Effects of diagonal crack angle on bulging of cover surface (f_t = 2.5 MPa, $E_{c,ef}$ = 20 GPa, c = 25 mm, D = 16 mm, d_0 = 12.5 μm, β = 3, $d_{s,max}$ = 50 μm)

Fig. 12 shows a comparison of the crack mouth opening displacement of the diagonal crack and surface crack at the same corroded thickness. It can be found that the crack mouth opening displacement of the diagonal crack can be wider or narrower than the crack mouth opening displacement of the surface crack at different diagonal crack angles.

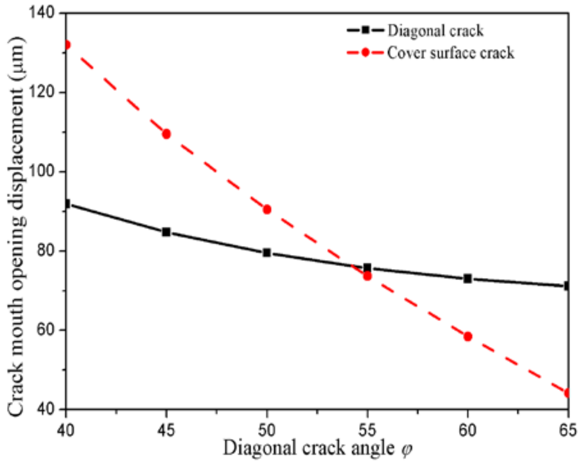

Fig. 12 Effects of diagonal crack angle on crack mouth opening displacement (f_t = 2.5 MPa, $E_{c,ef}$ = 20 GPa, c = 25 mm, D = 16 mm, d_0 = 12.5 μm, β = 3, $d_{s,max}$ = 50 μm)

5.2 Effect of tensile strength of concrete

The effect of the tensile strength of concrete is outlined in this section. The mechanical properties of concrete with different tensile strengths obtained from Chen and Su [81] are presented in Table 2. Using these properties, the variations in initiating and widening the diagonal crack and cover surface crack at the maximum thickness of the corroded steel for different tensile strengths of concrete are determined. The normalized crack widths of $CMOD_I/w_c$ and $CMOD_A/w_c$ are shown in Figs. 13a and 13b, respectively. The figures show that the maximum thickness of the corroded steel increases with an increase in the tensile strength of the concrete for the initiation of both the diagonal crack and cover surface crack. This is reasonable as concrete with a higher tensile strength results in a higher maximum thickness of the corroded rebar which initiates cracking in the concrete. With an increase in the maximum thickness of the corroded steel, it is also found that the maximum thickness of the corroded steel for a concrete tensile strength of 3.3 MPa (f_{cu} = 62.2 MPa) is more than that for a concrete tensile strength of 2.5 MPa (f_{cu} = 39.7 MPa) to develop the same normalized width of the diagonal crack (or same normalized width of the cover surface crack). The reason is because for concrete with normal strength (f_{cu} < 60 MPa), a larger tensile strength (together with a higher Young's modulus) requires a higher maximum thickness of the corroded steel to produce the same normalized crack width. However, for the same normalized width of the diagonal crack (or same normalized width of the cover surface crack), the maximum thickness of the corroded steel for a concrete tensile strength of 4.5 MPa is smaller for a concrete tensile strength of 3.3 MPa and even smaller for a concrete tensile strength of 2.5 MPa. This is because concrete with such a high tensile strength (4.5 MPa) is a high-strength concrete (f_{cu} = 80.5 MPa) which exhibits much more brittle behavior than normal strength concrete.

Table 2 Mechanical properties of concrete

$E_{c,ef}$ (GPa)	f_{cu} (MPa)	f_t (MPa)	w_c (μm)
21	39.7	2.5	214
23	62.2	3.3	238.3
29	80.5	4.5	188.7

Note: f_{cu} is the compressive strength of concrete; w_c is the crack width when residual tensile stress of concrete is equal to 0.

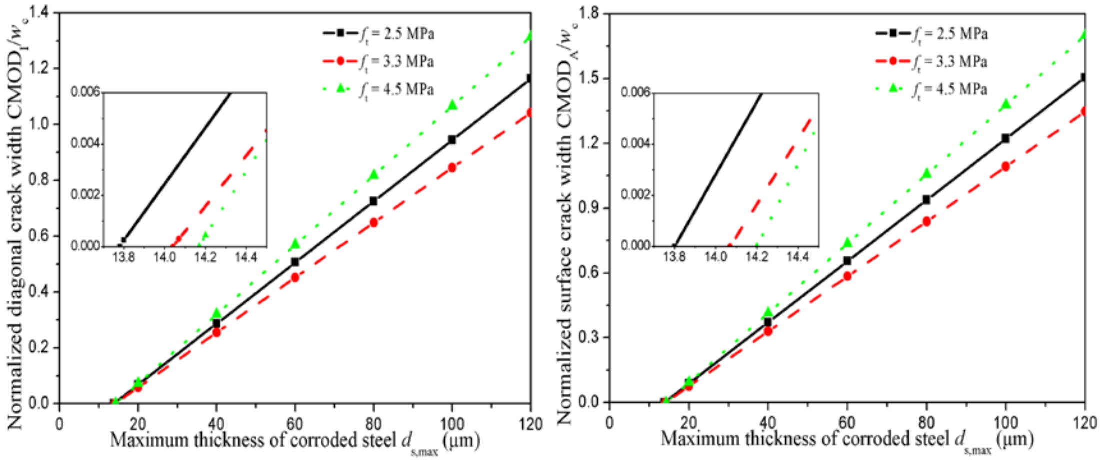

(a) Diagonal crack (b) Cover surface crack

Fig. 13 Effects of tensile strength of concrete on maximum corroded thickness of rebar for initiating and widening (a) diagonal crack and (b) cover surface crack (c = 25 mm, D = 16 mm, d_0 = 12.5 μm, β = 3, φ = 45°)

5.3 Effects of cover thickness

Fig. 14 shows the effects of cover thickness on the maximum thickness of the corroded steel for initiating and widening the diagonal crack and cover surface crack. Fig. 14a shows the variation of CMOD$_I$ with cover thickness. It is interesting to see that the maximum thickness of the corroded steel to initiate the diagonal crack decreases with an increase in cover thickness while the CMOD$_I$ increases as the cover thickness is increased for the same thickness of the corroded rebar. This is reasonable as a thicker cover inhibits the initiation of corrosion. However, the maximum thickness of the corroded steel that will initiate a diagonal crack will be smaller for a thicker cover, and later on, the crack width is greater with the same thickness of corroded steel.

Fig. 14b shows the effect of the cover thickness on the maximum thickness of the corroded steel for initiating and widening the surface crack. It can be observed that a greater cover thickness results in a thicker corroded steel required for initiating cracking which concurs with the numerical findings in Zhang et al. [29] and Cui and Alipour

[49]. However, the width of the cover surface crack on a thicker cover increases faster and could be greater than that of a thinner cover, which is supported by the results in Chen and Leung [26].

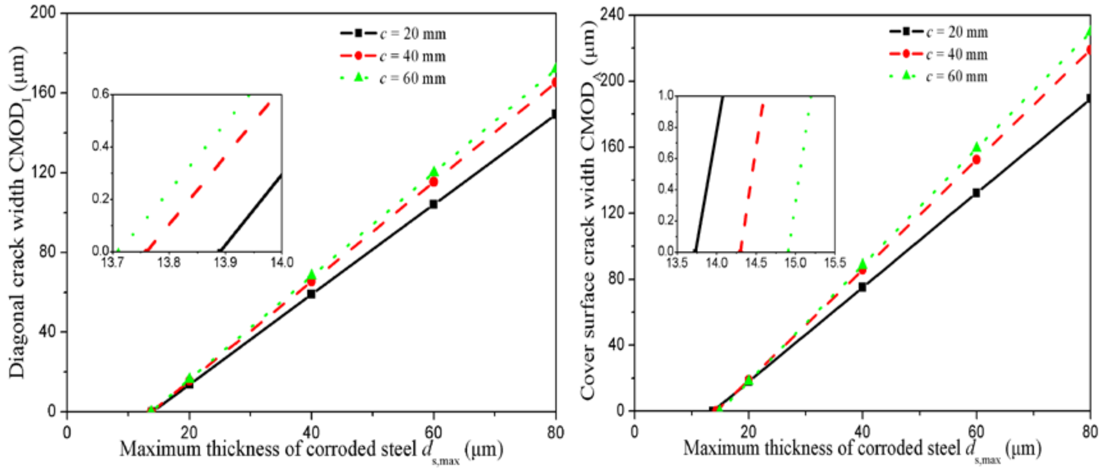

(a) Diagonal crack (b) Cover surface crack

Fig. 14 Effects of cover thickness on maximum corroded thickness of rebar for initiating and widening (a) diagonal crack; (b) cover surface crack (f_t = 2.5 MPa, $E_{c,ef}$ = 20 GPa, D = 16 mm, d_0 = 12.5 μm, β = 3, φ = 45°)

5.4 Variations in deformation of cover surface

Fig. 15 shows the variations in the bulging of the cover surface with a maximum thickness of the corroded rebar. It can be seen that the deformation of the cover surface increases with an increase in the maximum thickness of the corroded steel. This observation is supported by the work in Tran et al. [34].

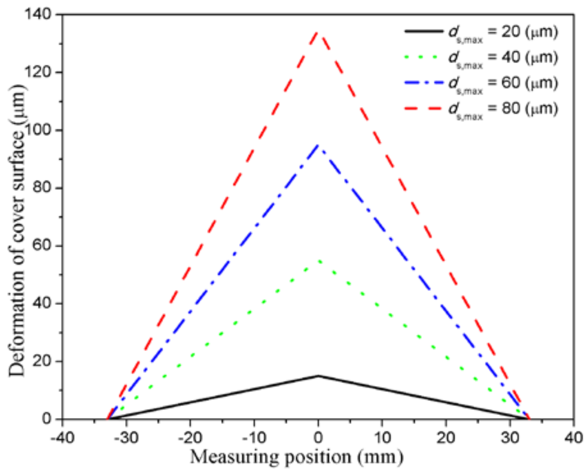

Fig. 15 Variations in deformation of cover surface with maximum thickness of corroded steel (f_t = 2.5 MPa, $E_{c,ef}$ = 20 GPa, c = 25 mm, D = 16 mm, d_0 = 12.5 μm, β = 3, φ = 45°)

6. Conclusions

In this study, an EBR model is proposed to analyze concrete cover spalling due to the non-uniform corrosion of widely-spaced multiple rebars. The following conclusions are made as a result.

(1) The mechanism and the process of cover cracking and spalling caused by the non-uniform corrosion of rebars have been analyzed and elaborated, and validated by using finite element modeling and available experimental results.

(2) The maximum thickness of the corroded steel for initiating and widening diagonal cracks and cover surface cracks can be obtained directly from this model. The relationships among the maximum thickness of the corroded steel, crack mouth opening displacement of the diagonal and surface cracks and the bulging of the cover surface can be determined by using the EBR model, which will allow engineers, designers and researchers to predict the amount of corrosion in rebars and width of internal diagonal cracks based on the measured crack mouth opening displacement of surface cracks or bulging of the cover surface.

(3) The bulging of the concrete cover obtained by using the EBR model is verified through a comparison with the experimental and numerical results qualitatively and quantitatively. This study demonstrates that the proposed model can be used to predict the bulging of concrete cover induced by rebar corrosion.

(4) The effects of the diagonal cracking angle, tensile strength of concrete and cover thickness on the bulging of the concrete cover, maximum thickness of the corroded steel for initiating and widening diagonal or cover surface cracks have been presented. It is found that the diagonal cracking angle has a major influence on the cover surface crack width when using the EBR model to predict the corrosion degree of rebar and the residual service life of RC structures. More field and experimental studies should be conducted to investigate the factors which can affect the diagonal cracking angle.

Acknowledgements

The research carried out in this paper gratefully acknowledges financial support from the Seed Fund for Basic Research of The University of Hong Kong.

Data availability statement

The raw/processed data required to validate the results have been presented in the paper. No further data can be shared at this time.

References

[1] K. Bhargava, A.K. Ghosh, Y. Mori, S. Ramanujam, Model for cover cracking due to rebar corrosion in RC structures, Engineering Structures 28(8) (2006) 1093-1109.

[2] Y. Liu, R. Weyers, Modeling the time-to-corrosion cracking in chloride contaminated reinforced concrete structures, ACI Materials Journal 95(6) (1998) 675-681.
[3] R.K.L. Su, Y. Zhang, A double-cylinder model incorporating confinement effects for the analysis of corrosion-caused cover cracking in reinforced concrete structures, Corrosion Science 99 (2015) 205-218.
[4] F. Chen, H. Baji, C.-Q. Li, A comparative study on factors affecting time to cover cracking as a service life indicator, Construction and Building Materials 163 (2018) 681-694.
[5] Y. Zhao, J. Yu, W. Jin, Damage analysis and cracking model of reinforced concrete structures with rebar corrosion, Corrosion Science 53(10) (2011) 3388-3397.
[6] Y. Ma, Z. Guo, L. Wang, J. Zhang, Experimental investigation of corrosion effect on bond behavior between reinforcing bar and concrete, Construction and Building Materials 152 (2017) 240-249.
[7] Y. Du, M. Cullen, C. Li, Structural performance of RC beams under simultaneous loading and reinforcement corrosion, Construction and Building Materials 38 (2013) 472-481.
[8] J. Dong, Y. Zhao, K. Wang, W. Jin, Crack propagation and flexural behaviour of RC beams under simultaneous sustained loading and steel corrosion, Construction and Building Materials 151 (2017) 208-219.
[9] A. Dasar, H. Hamada, Y. Sagawa, D. Yamamoto, Deterioration progress and performance reduction of 40-year-old reinforced concrete beams in natural corrosion environments, Construction and Building Materials 149 (2017) 690-704.
[10] D. Li, R. Wei, F. Xing, L. Sui, Y. Zhou, W. Wang, Influence of non-uniform corrosion of steel bars on the seismic behavior of reinforced concrete columns, Construction and Building Materials 167 (2018) 20-32.
[11] B. Sanz, J. Planas, J.M. Sancho, Study of the loss of bond in reinforced concrete specimens with accelerated corrosion by means of push-out tests, Construction and Building Materials 160 (2018) 598-609.
[12] H. Ye, C. Fu, N. Jin, X. Jin, Performance of reinforced concrete beams corroded under sustained service loads: A comparative study of two accelerated corrosion techniques, Construction and Building Materials 162 (2018) 286-297.
[13] C. Andrade, A. Cesetti, G. Mancini, F. Tondolo, Estimating corrosion attack in reinforced concrete by means of crack opening, Structural Concrete 17(4) (2016) 533-540.
[14] Y. Yuan, Y. Ji, Modeling corroded section configuration of steel bar in concrete structure, Construction and Building Materials 23(6) (2009) 2461-2466.
[15] C.A. Apostolopoulos, S. Demis, V.G. Papadakis, Chloride-induced corrosion of

steel reinforcement – Mechanical performance and pit depth analysis, Construction and Building Materials 38 (2013) 139-146.

[16] W. Zhu, R. François, Y. Liu, Propagation of corrosion and corrosion patterns of bars embedded in RC beams stored in chloride environment for various periods, Construction and Building Materials 145 (2017) 147-156.

[17] Y. Zhao, B. Hu, J. Yu, W. Jin, Non-uniform distribution of rust layer around steel bar in concrete, Corrosion Science 53(12) (2011) 4300-4308.

[18] C. Andrade, P. Garcés, I. Martínez, Galvanic currents and corrosion rates of reinforcements measured in cells simulating different pitting areas caused by chloride attack in sodium hydroxide, Corrosion Science 50(10) (2008) 2959-2964.

[19] B. Elsener, Macrocell corrosion of steel in concrete – implications for corrosion monitoring, Cement and Concrete Composites 24(1) (2002) 65-72.

[20] C.M. Hansson, A. Poursaee, A. Laurent, Macrocell and microcell corrosion of steel in ordinary Portland cement and high performance concretes, Cement and Concrete Research 36(11) (2006) 2098-2102.

[21] S. Qian, J. Zhang, D. Qu, Theoretical and experimental study of microcell and macrocell corrosion in patch repairs of concrete structures, Cement and Concrete Composites 28(8) (2006) 685-695.

[22] M. Raupach, Chloride-induced macrocell corrosion of steel in concrete—theoretical background and practical consequences, Construction and Building Materials 10(5) (1996) 329-338.

[23] K.V. Subramaniam, M. Bi, Investigation of steel corrosion in cracked concrete: evaluation of macrocell and microcell rates using Tafel polarization response, Corrosion Science 52(8) (2010) 2725-2735.

[24] X. Zhu, G. Zi, A 2D mechano-chemical model for the simulation of reinforcement corrosion and concrete damage, Construction and Building Materials 137 (2017) 330-344.

[25] C. Cao, M.M.S. Cheung, Non-uniform rust expansion for chloride-induced pitting corrosion in RC structures, Construction and Building Materials 51 (2014) 75-81.

[26] E. Chen, C.K.Y. Leung, Finite element modeling of concrete cover cracking due to non-uniform steel corrosion, Engineering Fracture Mechanics 134 (2015) 61-78.

[27] D. Qiao, H. Nakamura, Y. Yamamoto, T. Miura, Crack patterns of concrete with a single rebar subjected to non-uniform and localized corrosion, Construction and Building Materials 116 (2016) 366-377.

[28] B.S. Jang, B.H. Oh, Effects of non-uniform corrosion on the cracking and service life of reinforced concrete structures, Cement and Concrete Research 40(9) (2010) 1441-1450.

[29] J. Zhang, X. Ling, Z. Guan, Finite element modeling of concrete cover crack

propagation due to non-uniform corrosion of reinforcement, Construction and Building Materials 132 (2017) 487-499.

[30] Y. Zhao, X. Zhang, H. Ding, W. Jin, Non-uniform distribution of a corrosion layer at a steel/concrete interface described by a Gaussian model, Corrosion Science 112 (2016) 1-12.

[31] Y. Zhao, A.R. Karimi, H.S. Wong, B. Hu, N.R. Buenfeld, W. Jin, Comparison of uniform and non-uniform corrosion induced damage in reinforced concrete based on a Gaussian description of the corrosion layer, Corrosion Science 53(9) (2011) 2803-2814.

[32] S. Muthulingam, B.N. Rao, Non-uniform time-to-corrosion initiation in steel reinforced concrete under chloride environment, Corrosion Science 82 (2014) 304-315.

[33] X. Du, L. Jin, R. Zhang, Modeling the cracking of cover concrete due to non-uniform corrosion of reinforcement, Corrosion Science 89 (2014) 189-202.

[34] K.K. Tran, H. Nakamura, K. Kawamura, M. Kunieda, Analysis of crack propagation due to rebar corrosion using RBSM, Cement and Concrete Composites 33(9) (2011) 906-917.

[35] B. Šavija, M. Luković, J. Pacheco, E. Schlangen, Cracking of the concrete cover due to reinforcement corrosion: A two-dimensional lattice model study, Construction and Building Materials 44 (2013) 626-638.

[36] S. Muthulingam, B.N. Rao, Non-uniform corrosion states of rebar in concrete under chloride environment, Corrosion Science 93 (2015) 267-282.

[37] T. Pan, Y. Lu, Stochastic modeling of reinforced concrete cracking due to nonuniform corrosion: FEM-based cross-scale analysis, Journal of Materials in Civil Engineering 24(6) (2012) 698-706.

[38] C. Cao, 3D simulation of localized steel corrosion in chloride contaminated reinforced concrete, Construction and Building Materials 72 (2014) 434-443.

[39] C.Y. Kim, J.K. Kim, Numerical analysis of localized steel corrosion in concrete, Construction and Building Materials 22(6) (2008) 1129-1136.

[40] N. Xia, Q. Ren, R.Y. Liang, J. Payer, A. Patnaik, Nonuniform corrosion-induced stresses in steel-reinforced concrete, Journal of Engineering Mechanics 138(4) (2012) 338-346.

[41] E. Chen, C.K.Y. Leung, A coupled diffusion-mechanical model with boundary element method to predict concrete cover cracking due to steel corrosion, Corrosion Science 126 (2017) 180-196.

[42] X. Xi, S. Yang, C.-Q. Li, A non-uniform corrosion model and meso-scale fracture modelling of concrete, Cement and Concrete Research 108 (2018) 87-102.

[43] A. Bossio, T. Monetta, F. Bellucci, G.P. Lignola, A. Prota, Modeling of concrete cracking due to corrosion process of reinforcement bars, Cement and Concrete Research 71 (2015) 78-92.

[44] E. Chen, C.K.Y. Leung, Mechanical aspects of simulating crack propagation in concrete under steel corrosion, Construction and Building Materials 191 (2018) 165-175.
[45] J. Ožbolt, G. Balabanić, M. Kušter, 3D Numerical modelling of steel corrosion in concrete structures, Corrosion Science 53(12) (2011) 4166-4177.
[46] J.P. Callahan, J.L. Lott, C.E. Kesler, Bridge deck deterioration and crack control, Journal of the Structural Division 96(10) (1970) 2021-2036.
[47] Z.P. Bazant, Physical model for steel corrosion in concrete sea structures-application, ASCE J Struct Div 105(6) (1979) 1155-1166.
[48] X. Xi, S. Yang, Time to surface cracking and crack width of reinforced concrete structures under corrosion of multiple rebars, Construction and Building Materials 155 (2017) 114-125.
[49] Z. Cui, A. Alipour, Concrete cover cracking and service life prediction of reinforced concrete structures in corrosive environments, Construction and Building Materials 159 (2018) 652-671.
[50] S. Guzmán, J.C. Gálvez, Modelling of concrete cover cracking due to non-uniform corrosion of reinforcing steel, Construction and Building Materials 155 (2017) 1063-1071.
[51] K. Vu, M. Stewart, J. Mullard, Corrosion-induced cracking: experimental data and predictive models, ACI Structural Journal 102(5) (2005) 719-726.
[52] A. Jamali, U. Angst, B. Adey, B. Elsener, Modeling of corrosion-induced concrete cover cracking: A critical analysis, Construction and Building Materials 42 (2013) 225-237.
[53] S. Caré, Q. Nguyen, K. Beddiar, Y. Berthaud, Times to cracking in reinforced mortar beams subjected to accelerated corrosion tests, Materials and Structures 43(1-2) (2010) 107-124.
[54] C. Fahy, S.J. Wheeler, D. Gallipoli, P. Grassl, Corrosion induced cracking modelled by a coupled transport-structural approach, Cement and Concrete Research 94(C) (2017) 24-35.
[55] C. Fahy, D. Gallipoli, S.J. Wheeler, P. Grassl, Transport-structural modelling of corrosion induced cracking, in: V. Saouma, J. Bolander, E. Landis (Eds.) 9th International Conference on Fracture Mechanics of Concrete and Concrete Structures, University of California, Berkeley, California USA, 2016.
[56] K. Kim, S. Jang, B. Jang, B. Oh, Modeling mechanical behavior of reinforced concrete due to corrosion of steel bar, ACI Materials Journal 107(2) (2010) 106-113.
[57] Y. Zhao, Y. Wu, W. Jin, Distribution of millscale on corroded steel bars and penetration of steel corrosion products in concrete, Corrosion Science 66 (2013) 160-168.

[58] H.M. Shodja, K. Kiani, A. Hashemian, A model for the evolution of concrete deterioration due to reinforcement corrosion, Mathematical and Computer Modelling 52(9-10) (2010) 1403-1422.
[59] K. Kiani, H.M. Shodja, Prediction of the penetrated rust into the microcracks of concrete caused by reinforcement corrosion, Applied Mathematical Modelling 35(5) (2011) 2529-2543.
[60] S.J. Jaffer, C.M. Hansson, Chloride-induced corrosion products of steel in cracked-concrete subjected to different loading conditions, Cement and Concrete Research 39(2) (2009) 116-125.
[61] H.S. Wong, Y.X. Zhao, A.R. Karimi, N.R. Buenfeld, W.L. Jin, On the penetration of corrosion products from reinforcing steel into concrete due to chloride-induced corrosion, Corrosion Science 52(7) (2010) 2469-2480.
[62] S.J. Pantazopoulou, K.D. Papoulia, Modeling cover-cracking due to reinforcement corrosion in RC structures, Journal of Engineering Mechanics 127(4) (2001) 342-351.
[63] J. Ožbolt, F. Oršanić, G. Balabanić, M. Kušter, Modeling damage in concrete caused by corrosion of reinforcement: coupled 3D FE model, International Journal of Fracture 178(1) (2012) 233-244.
[64] Y. Zhao, J. Yu, Y. Wu, W. Jin, Critical thickness of rust layer at inner and out surface cracking of concrete cover in reinforced concrete structures, Corrosion Science 59 (2012) 316-323.
[65] Y. Zhao, H. Ren, H. Dai, W. Jin, Composition and expansion coefficient of rust based on X-ray diffraction and thermal analysis, Corrosion Science 53(5) (2011) 1646-1658.
[66] B. Sanz, J. Planas, J.M. Sancho, A method to determine the constitutive parameters of oxide in accelerated corrosion tests of reinforced concrete specimens, Cement and Concrete Research 101 (2017) 68-81.
[67] B. Sanz, J. Planas, J.M. Sancho, A closer look to the mechanical behavior of the oxide layer in concrete reinforcement corrosion, International Journal of Solids and Structures 62(C) (2015) 256-268.
[68] T. El Maaddawy, K. Soudki, A model for prediction of time from corrosion initiation to corrosion cracking, Cement and Concrete Composites 29(3) (2007) 168-175.
[69] U. Angst, M. Geiker, A. Michel, C. Gehlen, H. Wong, O. Isgor, B. Elsener, C. Hansson, R. François, K. Hornbostel, R. Polder, M. Alonso, M. Sanchez, M. Correia, M. Criado, A. Sagüés, N. Buenfeld, The steel–concrete interface, Materials and Structures 50(2) (2017) 1-24.
[70] C. Lu, W. Jin, R. Liu, Reinforcement corrosion-induced cover cracking and its time prediction for reinforced concrete structures, Corrosion Science 53(4) (2011) 1337-

1347.
[71] D.V. Val, L. Chernin, M.G. Stewart, Experimental and numerical investigation of corrosion-induced cover cracking in reinforced concrete structures, Journal of Structural Engineering 135(4) (2009) 376-385.
[72] Y. Zhao, H. Ding, W. Jin, Development of the corrosion-filled paste and corrosion layer at the steel/concrete interface, Corrosion Science 87 (2014) 199-210.
[73] Y. Zhao, J. Dong, Y. Wu, W. Jin, Corrosion-induced concrete cracking model considering corrosion product-filled paste at the concrete/steel interface, Construction and Building Materials 116 (2016) 273-280.
[74] L. Chernin, D. Val, K. Volokh, Analytical modelling of concrete cover cracking caused by corrosion of reinforcement, Materials and Structures 43(4) (2010) 543-556.
[75] L. Chernin, D. Val, M. Stewart, Prediction of cover crack propagation in RC structures caused by corrosion, Magazine of Concrete Research 64(2) (2012) 95-111.
[76] F.J. Molina, C. Alonso, C. Andrade, Cover cracking as a function of rebar corrosion: Part 2—Numerical model, Materials and Structures 26(9) (1993) 532-548.
[77] I. Balafas, C.J. Burgoyne, Environmental effects on cover cracking due to corrosion, Cement and Concrete Research 40(9) (2010) 1429-1440.
[78] Y. Zhao, H. Dai, H. Ren, W. Jin, Experimental study of the modulus of steel corrosion in a concrete port, Corrosion Science 56 (2012) 17-25.
[79] A. Bossio, G.P. Lignola, F. Fabbrocino, T. Monetta, A. Prota, F. Bellucci, G. Manfredi, Nondestructive assessment of corrosion of reinforcing bars through surface concrete cracks, Structural Concrete 18(1) (2017) 104-117.
[80] S.A. Mirza, M. Hatzinikolas, J.G. MacGregor, Statistical descriptions of strength of concrete, Journal of the Structural Division 105(6) (1979) 1021-1037.
[81] H.H. Chen, R.K.L. Su, Tension softening curves of plain concrete, Construction and Building Materials 44 (2013) 440-451.